Hindawi
Mathematical Problems in Engineering
Volume 2017, Article ID 7027016, 15 pages
https://doi.org/10.1155/2017/7027016

Research Article

Derivation of the Mathematical Approach to the Radial Pump's Meridional Channel Design Based on the Controlment of the Medial Axis

Yeming Lu,[1,2] Xiaofang Wang,[1,2] and Rong Xie[1,2]

[1]*School of Energy and Power Engineering, Dalian University of Technology, Dalian 116000, China*
[2]*Collaborative Innovation Center of Major Machine Manufacturing in Liaoning, Dalian 116000, China*

Correspondence should be addressed to Xiaofang Wang; dlwxf@dlut.edu.cn

Received 16 May 2017; Revised 9 July 2017; Accepted 1 August 2017; Published 19 October 2017

Academic Editor: Renata Archetti

The meridional channel is the base for designing the radial pumps, and a new design approach is proposed here. Different from the previous studies, research here tries to establish the design model simply controlled with the radial coordinate. With the combination of a series of mathematical equations, the new design approach can shape the meridional contours directly by using the initial design variables. As for the mathematical constraint in the new design approach, it was presented in two forms, and each form had its corresponding solution. For the first form (*Constraint I*), the midpoints of the design points on the hub and shroud contours were thought to be located on the medial axis, and the PSO algorithm was adopted to search for the suitable results. Continually, to accelerate the design process, the second form (*Constraint II*) to simplify the mathematical constraint was added, and the explicit mathematical expressions calculating the coordinates on the hub and shroud contours were deduced. Finally, to check out the feasibility of the design approach in engineering, it was applied to redesign some typical meridional channels proposed by previous studies, and, through comparative analysis, the effectiveness of the new approach was evaluated and demonstrated.

1. Introduction

Radial pumps mainly consist of the centrifugal pump and the mixed-flow pump [1], which are widely applied in various areas such as the chemical industry, the industrial water applications, and the nuclear industry [2]. As the heart of the power equipment in these related areas, the pumps could provide stable energy for the circulation of fluid medium. The need for designing a higher efficiency pump consuming lower energy is increasing with the advocacy for green power, nowadays [3]. Hence, an effective design method for configuring the pump with high performance would be significant [4]. To design the pump, two aspects, namely, the blade shape and the meridional channel, can be considered [5]. Though many inverse design methods about the blade shape have already been conducted by former studies [6–8], little attention has been paid to the meridional channel design. Nevertheless, the meridional shape is the foundation for the pump design, and Bing et al. [9] had proven that the meridional shape has great effects on the pump performance, so that the related design method about the meridional channel should be treated seriously.

In terms of the meridional channel design approach, Casey [10] used the Bezier curves to design the hub and shroud contours of the pump, but it is hard to guarantee the good flow characteristics on the cross sections due to the nonsynchronicity design of the hub and shroud contours. Additionally, minor adjustment of the control points on the Bezier curves can lead to a wide change of the meridional shape, which is not useful for local modification and optimization, sometimes. Apart from the shortcomings in optimization, the Bezier curves may confront troubles in the preliminary design of the meridional shape; for that the control points on the Bezier curves are just given according to the expert experience without too much consideration of the related mathematical constraints in most of the conditions.

Based on the ISO 2858-1975 standard, Guan [11] used many linear lines and circular arcs to design the meridional shapes of some industrial centrifugal pumps, and they are widely used in China due to the good anticavitation property and simple structure. Nevertheless, as for this traditional design method, a large amount of tests have to be done to settle down the specific values determining the arcs and lines. When faced with the new design requirement beyond the previous design cases, this traditional meridional design method cannot give the specific procedures to identify the design parameters except for the abundant tests, which is rather time-consuming. Moreover, apart from the application in the centrifugal pump design area, the traditional design method is not so popularized in the mixed-flow pump design; therefore, there is a lack of a united design approach to design the meridional shape of the centrifugal pump and the mixed-flow pump.

Instead of geometrically designing the meridional channel with linear lines and circular arcs, an important medial axis transform theory was firstly proposed by Choi et al. [12], which was subsequently extended to meridional shape design by Zou et al. [13] and Wang et al. [14]. In succession, Wang et al. [15] adopted the medial axis method in his study and had designed the meridional shapes with different inlet conditions. However, in terms of the previous meridional design approach transformed with the medial axis, too much variables are adopted to design the meridional channel with the complex constrained equations, and among these design variables, the main determined variables are not so clear, which is not beneficial for further modification and optimization.

Although it can be concluded that former studies have already done relevant works, there are still some challenges waiting to be solved; consequently, the new meridional channel design approach making up for the partial shortcomings of the previous design methods is proposed in this study. In comparison with the previous methods, the proposed design approach has many advantages. Firstly, it provides a united way to design the meridional channel of the centrifugal pump as well as the mixed-flow pump, which would be verified in the design cases of this study. Secondly, taking the rigid mathematical constraints guaranteeing the good hydraulic characteristics into consideration, the proposed design approach selects the radial coordinate as the single control variable, which is much more simple and manipulable. Moreover, instead of the complex implicit equations, simpler explicit expressions are in great demand in engineering, and an explicit design formula is proposed in the new design approach according to the simplified condition (*Constraint II* in Section 3.3). Last but not least, the proposed design approach could design the meridional shape including the hub, the medial axis, and the shroud contours directly, which would provide the skeleton and structural parameters for the inverse design of the blade, and this would be further discussed in Section 6.2. Plus, the new meridional shape design approach can also help to extend the design theory of the pump.

Taking the envelope formula of the medial axis transform (MAT) theory [12–15] into consideration, research here transformed it into another simple manner controlled by the independent variable of the radial coordinate. Then based on the transformed envelope formula, the circular equation, and the cross section area equation, two kinds of mathematical constraints which had the corresponding solutions for the shape design were introduced. For the first constraint *(Constraint I)*, the partial swarm optimization (PSO) algorithm was adopted to search for the suitable points in the design process. And for the second one *(Constraint II)*, the deduced mathematical expressions calculating the coordinates on the hub and shroud contours were presented. Finally, the design method was applied to redesign the typical meridional shapes, and its effectiveness was verified by comparison with the previous design. The paper is organized as follows: Section 2 gives the details of the basic design theory; in particular, the simplification process for the envelope formula in MAT theory is given. Section 3 describes the mathematical constraints and gives the corresponding solution for the meridional channel design. Section 4 shows the design results of the typical structures. Section 5 analyzes the design results and explores the possibilities of the new design approach in other design conditions. Section 6 provides the conclusions and future work.

2. Basic Design Theories

2.1. Simplification of Envelope Formula in MAT Theory. The medial axis transform (MAT) method was firstly proposed by Blum [17] to recognize the biological shape, and then it was extended to various areas, for example, the finite-element meshing [18] and the pattern recognition [19]. To calculate the cross section areas and adjust the hub and shroud contours conveniently, the MAT theory was adopted here to design the meridional channel of the radial pump. The enveloping formula in the MAT method is given as [12]

$$\begin{aligned}\mathbf{S}(t) &= \mathbf{M}(t) \\ &\quad + d(t)\left\{-d'(t)\,\mathbf{p}(t) + \sqrt{1-\left(d'(t)\right)^2}\,\mathbf{q}(t)\right\} \\ \mathbf{H}(t) &= \mathbf{M}(t) \\ &\quad + d(t)\left\{-d'(t)\,\mathbf{p}(t) - \sqrt{1-\left(d'(t)\right)^2}\,\mathbf{q}(t)\right\},\end{aligned} \tag{1}$$

where t denotes the location in the natural coordinate; $d(t)$ is the radius of the inscribed circle; $\mathbf{p}(t)$ denotes the tangent vector, whose norm is 1; and $\mathbf{q}(t)$ represents the vector which is perpendicular to $\mathbf{p}(t)$, and its norm equals 1, too.

Continually, different from the previous studies [13–15], research here would use the radial coordinate r to take the place of the natural coordinate t; thus, r becomes the independent variable in the envelope formula of the MAT theory. Comparatively, $d(t)$, $\mathbf{p}(t)$, $\mathbf{q}(t)$, and $z(t)$ in Figure 1 can be replaced with $d(r)$, $\mathbf{p}(r)$, $\mathbf{q}(r)$, and $z(r)$. As a result, based on these separate changes, the details of the transformation process for envelope formula (see (1)) would be presented next.

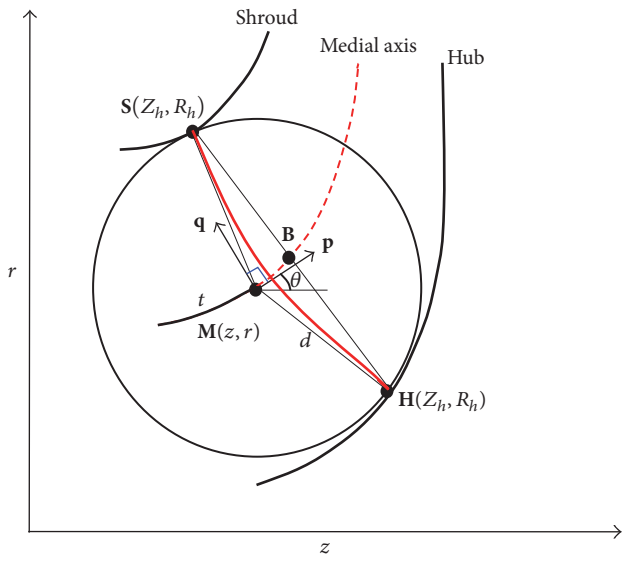

FIGURE 1: Sketch representation of the MAT.

As shown in Figure 1, the tangent of θ can be calculated as

$$\tan\theta = \frac{dr}{dz} = \frac{1}{(dz/dr)} = \frac{1}{z'(r)}. \tag{2}$$

Consequently, $\mathbf{p}(t)$ and $\mathbf{q}(t)$ in (1) can be expressed as

$$\mathbf{p}(t) = \begin{pmatrix} \cos\theta \\ \sin\theta \end{pmatrix} = \begin{pmatrix} \dfrac{z'(r)}{\sqrt{1+(z'(r))^2}} \\ \dfrac{1}{\sqrt{1+(z'(r))^2}} \end{pmatrix},$$
$$\mathbf{q}(t) = \begin{pmatrix} -\sin\theta \\ \cos\theta \end{pmatrix} = \begin{pmatrix} \dfrac{-1}{\sqrt{1+(z'(r))^2}} \\ \dfrac{z'(r)}{\sqrt{1+(z'(r))^2}} \end{pmatrix}. \tag{3}$$

Next, $d'(t)$ can be deduced as

$$d'(t) = \frac{dd}{dt} = \frac{dd}{\sqrt{(dz)^2+(dr)^2}} = \frac{dd}{\sqrt{1+(z'(r))^2}dr} = \frac{1}{\sqrt{1+(z'(r))^2}}d'(r). \tag{4}$$

With (2)~(4), (1) can be further expressed as

$$\begin{pmatrix} Z_s \\ R_s \end{pmatrix} = \begin{pmatrix} z(r) \\ r \end{pmatrix} + d(r)\left\{ -\frac{d'(r)}{\sqrt{1+(z'(r))^2}} \cdot \begin{pmatrix} \dfrac{z'(r)}{\sqrt{1+(z'(r))^2}} \\ \dfrac{1}{\sqrt{1+(z'(r))^2}} \end{pmatrix} + \frac{\sqrt{1-(z'(r))^2-(d'(r))^2}}{\sqrt{1+(z'(r))^2}} \cdot \begin{pmatrix} \dfrac{-1}{\sqrt{1+(z'(r))^2}} \\ \dfrac{z'(r)}{\sqrt{1+(z'(r))^2}} \end{pmatrix} \right\}$$
$$\begin{pmatrix} Z_h \\ R_h \end{pmatrix} = \begin{pmatrix} z(r) \\ r \end{pmatrix} + d(r)\left\{ -\frac{d'(r)}{\sqrt{1+(z'(r))^2}} \cdot \begin{pmatrix} \dfrac{z'(r)}{\sqrt{1+(z'(r))^2}} \\ \dfrac{1}{\sqrt{1+(z'(r))^2}} \end{pmatrix} - \frac{\sqrt{1-(z'(r))^2-(d'(r))^2}}{\sqrt{1+(z'(r))^2}} \cdot \begin{pmatrix} \dfrac{-1}{\sqrt{1+(z'(r))^2}} \\ \dfrac{z'(r)}{\sqrt{1+(z'(r))^2}} \end{pmatrix} \right\}. \tag{5}$$

Also, (5) can be further transformed as

$$Z_s = z(r) - \frac{d(r)d'(r)z'(r)}{1+(z'(r))^2} - \frac{\sqrt{1-(z'(r))^2-(d'(r))^2}}{1+(z'(r))^2},$$
$$R_s = r - \frac{d(r)d'(r)}{1+(z'(r))^2} + \frac{z'(r)\sqrt{1-(z'(r))^2-(d'(r))^2}}{1+(z'(r))^2},$$
$$Z_h = z(r) - \frac{d(r)d'(r)z'(r)}{1+(z'(r))^2} + \frac{\sqrt{1-(z'(r))^2-(d'(r))^2}}{1+(z'(r))^2}$$

$$R_h = r - \frac{d(r)\,d'(r)}{1+\left(z'(r)\right)^2} - \frac{z'(r)\sqrt{1-\left(z'(r)\right)^2-\left(d'(r)\right)^2}}{1+\left(z'(r)\right)^2}. \tag{6}$$

With the combination of (6), the final simplified envelop formula from the MAT theory can be expressed as

$$\begin{aligned} z'(r)\left[Z_s - z(r)\right] + \left(R_s - r\right) &= -d'(r)\,d(r), \\ z'(r)\left[Z_h - z(r)\right] + \left(R_h - r\right) &= -d'(r)\,d(r). \end{aligned} \tag{7}$$

From (7), it can be concluded out that the envelope formula has been successfully transformed into a simpler manner controlled by the independent variable r of the radial coordinate.

2.2. The Circular Equation. As for the enveloping circle shown in Figure 1, its center point is $\mathbf{M}(z(r), r)$, and the radius is $d(r)$. Thus, according to the circular equation, the mathematical relationships between the coordinates of **S** and **H** can be expressed as follows:

$$\left[Z_h - z(r)\right]^2 + \left(R_h - r\right)^2 = \left[d(r)\right]^2, \tag{8}$$

$$\left[Z_s - z(r)\right]^2 + \left(R_s - r\right)^2 = \left[d(r)\right]^2. \tag{9}$$

Similarly to (7), it is known that (8) and (9) from the circular equation are still controlled by the independent variable r of the radial coordinate, which would provide a united form for further simplification next.

2.3. The Cross Section Area Equation. As mentioned in Figure 1, the meridional channel is tangent to a series of enveloping circles, whose centers are located on the medial axis. For a random enveloping circle in the channel, it has a corresponding cross section arc. After rotating the cross section arc around the axial axis, the revolutionary surface called the cross section area can be generated. The cross section area $F(r)$ is an important variable, which can be calculated with the following equation [11]:

$$F(r) = 2\pi r_c b_c, \tag{10}$$

where r_c is center of the cross section arc and b_c denotes the length of the cross section arc. They can be settled down with the following formula:

$$\begin{aligned} r_c &= \frac{1}{3}\left(r + R_h + R_s\right) \\ b_c &= \frac{2}{3}\left\{d(r) + \sqrt{\left(Z_s - Z_h\right)^2 + \left(R_s - R_h\right)^2}\right\}, \end{aligned} \tag{11}$$

where $d(r)$ can be got from (8) or (9).

In [14, 15], the distribution of the cross section area $F(r)$ can be taken as a previous settled variable, so that the variable $F(r)$ can still be taken as a known variable before the meridional channel design in this study. However, in the other design conditions [13], the previous given cross section area $F(r)$ can also be replaced with some other design variables, for instance, the volume flow rate Q, the mean meridional velocity C_m, and the blockage factor τ, but actually, the distribution of $F(r)$ can be settled down previously with the following equation:

$$F(r) = \frac{Q}{C_m \tau}, \tag{12}$$

where C_m can be got from the simulation result or the experienced formula [14] ($C_m = A + Br$, where A and B are the constants determined by the inlet and outlet variables). τ is closed to 1 and can be ignored sometimes; moreover, it can also be calculated from some experienced formulas [11].

3. New Meridional Channel Design Approach Based on Different Mathematical Constraints

3.1. The Introduction of the Mathematical Constraint. As with previous studies [13, 14], the medial axis $(z(r), r)$ and the distribution of the cross section area $F(r)$ are chosen to be the prescribed design variables. And these known variables would be input to calculate the coordinates determining the meridional channel based on the basic design theories above. Next, the specific details for the calculation process are then to be presented.

In Figure 1, it is known that the meridional channel has been designed successfully after the settlement of the coordinates Z_s, R_s, Z_h, R_h, and these four variables should be in accord with the MAT theory, the circular equation, and the cross area equation set up in Section 2. To eliminate the irrelevant variables $d(r)$ and $d'(r)$, (7) got from the MAT theory can be preliminarily transformed as

$$\begin{aligned} &z'(r)\left[Z_s - z(r)\right] + \left(R_s - r\right) \\ &\quad = z'(r)\left[Z_h - z(r)\right] + \left(R_h - r\right). \end{aligned} \tag{13}$$

Accordingly, the circular equation can be expressed as

$$\left[Z_h - z(r)\right]^2 + \left(R_h - r\right)^2 = \left[Z_s - z(r)\right]^2 + \left(R_s - r\right)^2. \tag{14}$$

To represent Z_h, Z_s with other variables, (13) and (14) can be further transformed as

$$\begin{aligned} Z_h &= \frac{\left\{R_s - R_h + 2z(r)\,z'(r) + \left(R_s + R_h - 2r\right)\left[z'(r)\right]^2\right\}}{2z'(r)} \\ Z_s &= \frac{\left\{R_h - R_s + 2z(r)\,z'(r) + \left(R_s + R_h - 2r\right)\left[z'(r)\right]^2\right\}}{2z'(r)}. \end{aligned} \tag{15}$$

Moreover, from (8)–(11), the cross section area equation can be further deduced as

$$F(r) = \frac{4}{9}\pi(r + R_h + R_s)\left\{\sqrt{[Z_s - z(r)]^2 + (R_s - r)^2} + \sqrt{(Z_s - Z_h)^2 + (R_s - R_h)^2}\right\}. \quad (16)$$

So far, based on the basic design theory in Section 2, three equations (see (15) and (16)) are finally got to settle down the four variables Z_s, R_s, Z_h, R_h. Apparently, to close the calculation process, an extra equation is needed. Then two kinds of mathematical constraints got from different assumptions are imported to settle down the design variables.

3.2. Constraint I and the Solution with PSO Algorithm

3.2.1. Introduction of Constraint I. As shown in Figure 1, point **B** is the midpoint of point $\mathbf{S}(Z_s, R_s)$ and point $\mathbf{H}(Z_h, R_h)$. Since the distance between point **B** and point **M** is very small, the location of **B** can still be taken as on the prescribed medial axis. Therefore, the following mathematical constraint can be established as

$$\frac{Z_s + Z_h}{2} = z\left(\frac{R_s + R_h}{2}\right), \quad (17)$$

where $z((R_s + R_h)/2)$ can be calculated and got from the prescribed distribution of the medial axis $z(r)$ by the replacement of r with $(R_s + R_h)/2$.

To get the specific values of Z_s, R_s, Z_h, R_h, the PSO algorithm is imported to search for the right solution.

3.2.2. Applying PSO into the Calculation Process

(1) Establishment of the Objective Function. On the basis of the four established equations (see (15)~(17)), the values of Z_s, R_s, Z_h, R_h are then to be identified. In the calculation process, (16) and (17) can be expressed with Y_1, Y_2 as follows:

$$Y_1 = F(r) - \frac{4}{9}\pi(r + R_h + R_s) \cdot \left\{\sqrt{[Z_s - z(r)]^2 + (R_s - r)^2} + \sqrt{(Z_s - Z_h)^2 + (R_s - R_h)^2}\right\} = 0$$
$$Y_2 = \frac{Z_s + Z_h}{2} - z\left(\frac{R_s + R_h}{2}\right) = 0. \quad (18)$$

To connect the two equations in (18), an extra function $Y(Z_h, R_h, Z_s, R_s)$ is defined, and it is utilized to unite the two equations together as

$$Y(Z_h, R_h, Z_s, R_s) = -(|Y_1| + |Y_2|) = 0. \quad (19)$$

Up to now, for the suitable design variables Z_s, R_s, Z_h, R_h satisfying (16) and (17), they would also make the calculating result of $Y(Z_h, R_h, Z_s, R_s)$ in (19) equal to 0. Nevertheless, the maximum value of $Y(Z_h, R_h, Z_s, R_s)$ is just 0; namely, the corresponding variables Z_s, R_s, Z_h, R_h determining the maximum value will also make (16) and (17) true.

To find out the suitable variables Z_h, R_h, Z_s, R_s reaching the maximum value of $Y(Z_h, R_h, Z_s, R_s)$ and making (16) and (17) true, the PSO algorithm is adopted. Plus, if the constraints of (15) are also considered during the searching process, the calculated results would make (15)~(17) true; consequently, the meridional channel can be settled down with these calculated results. Therefore, the objective function can be established:

$$\begin{aligned}
&\max \quad Y(Z_h, R_h, Z_s, R_s) = -(|Y_1| + |Y_2|)\\
&\text{st.} \quad Z_h = \frac{\{R_s - R_h + 2z(r)z'(r) + (R_s + R_h - 2r)[z'(r)]\}}{2z'(r)}\\
&\qquad Z_s = \frac{\{R_h - R_s + 2z(r)z'(r) + (R_s + R_h - 2r)[z'(r)]\}}{2z'(r)}\\
&\qquad h_{\min} \le R_h \le h_{\max}\\
&\qquad s_{\min} \le R_s \le s_{\max}\\
&\qquad z \le \frac{Z_s + Z_h}{2},
\end{aligned} \quad (20)$$

where the variables r, $z(r)$, $z'(r)$ are from the prescribed variables; they are settled as the description of Fig S. 1 in APPENDIX A in Supplementary Material available online at https://doi.org/10.1155/2017/7027016; $h_{\min}$, $h_{\max}$, $s_{\min}$, $s_{\max}$ represent the search range of PSO in finding the suitable R_h, R_s, and to save the computing resource and shorten the search time (the search range can also be defined as a larger section, but it is time-consuming), they can be settled as

$$\begin{aligned}
h_{\min} &= r - \frac{b_1}{2}\\
h_{\max} &= r\\
s_{\min} &= r\\
s_{\max} &= r + \frac{b_1}{2},
\end{aligned} \quad (21)$$

where b_1 is the expected inlet width, which can be calculated from the given cross section area of the inlet.

(2) Solve the Objective Function with PSO Algorithm. PSO is firstly proposed by Kennedy and Eberhart [20] in 1995 according to the research on bird predation. As for the predation process, the easiest way to find food is to find out the partner who is nearest to the food. Inspired by this biological behavior, PSO is established and applied to solve the optimization problems. In the search space, the potential solutions called particles are assigned with a randomized velocity, a recorded coordinate, and a calculated best solution (fitness). The velocity determining the direction and distance of the particles' movement can be adjusted dynamically based

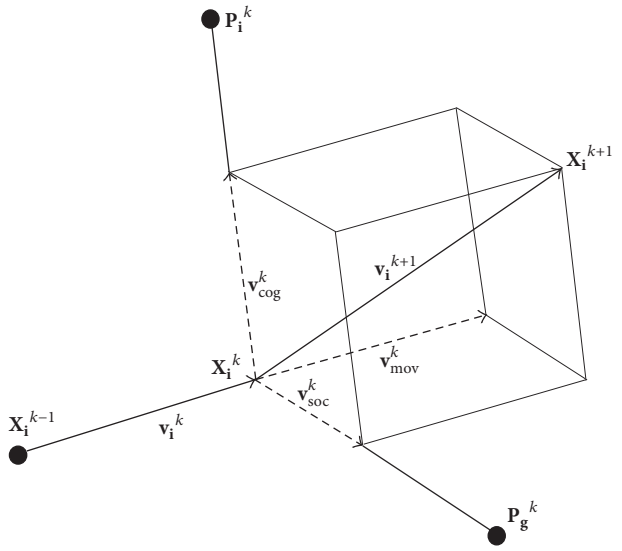

Figure 2: Movement of particles in the searching process.

on the moving experience. Each particle keeps record of the best solution called P_{best} and the related coordinates. At the same time, of all the particles so far in the population, the best solution called G_{best} in the global version is recorded, too. When the particles are updated at a time, P_{best} and G_{best} are also updated and reserved based on the newly calculated coordinates and fitness. This searching process is shown in Figure 2. For the movement of each particle, its velocity components mainly consist of the previous motion inertia, the social velocity, and the cognition velocity. The social velocity denotes the effects from the social members, which can be calculated from the distance between the local particle and the global best solution G_{best}. Similarly, the cognition velocity denotes the judgement of the particle itself in the searching process, and it can be calculated from the distance between the local particle and the best solution P_{best}. The calculations of the motion inertia, the social velocity, and the cognition velocity are all effectively conducted with (23) using the related real time-update parameters.

Assuming in the searching space of D dimensions, the population $\mathbf{X} = \{\mathbf{X_1}, \mathbf{X_2}, \ldots, \mathbf{X_n}\}$ consisted of n particles. As for the ith particle in the space it can be represented as $\mathbf{X_i} = (x_{i1}, x_{i2}, \ldots, x_{iD})^T$, which is on behalf of the potential solution. With the application of the objective function, the fitness value at location $\mathbf{X_i}$ can be calculated. In correspondence to $\mathbf{X_i}$, the search velocity is defined as $\mathbf{V_i} = (V_{i1}, V_{i2}, \ldots, V_{iD})^T$. Additionally, the coordinate of the corresponding P_{best} is $\mathbf{P_i} = (P_{i1}, P_{i2}, \ldots, P_{iD})^T$, and G_{best} is $\mathbf{P_g} = (P_{g1}, P_{g2}, \ldots, P_{gD})^T$. Similarly to the genetic algorithm, the PSO algorithm would find the optimal solution in the design space through a series of iterations. Thus, the $(k+1)$th step calculation is established on the calculation of the kth step, and the particles in Figure 2 update their positions and velocities with the following formulas:

$$\mathbf{X}^{k+1} = \mathbf{X}^k + \mathbf{v}^{k+1} \tag{22}$$

$$\begin{aligned}\mathbf{v}^{k+1} &= \mathbf{v}_{\text{mov}}^k + \mathbf{v}_{\text{soc}}^k + \mathbf{v}_{\text{cog}}^k \\ &= \omega(k)\,\mathbf{v_i}^k + c_1 m_1 \left(\mathbf{P_i}^k - \mathbf{X_i}^k\right) \\ &\quad + c_2 m_2 \left(\mathbf{P_g}^k - \mathbf{X_i}^k\right),\end{aligned} \tag{23}$$

where $\mathbf{v}_{\text{mov}}^k$, $\mathbf{v}_{\text{soc}}^k$, $\mathbf{v}_{\text{cog}}^k$ represent the motion inertia, the social velocity, and the cognition velocity, respectively; k is the iterative number, whose range is settled as $[1, 200]$ in this study; c_1, c_2 are the accelerate factors, which vary the contributions of personal best and local best attractors, and their values are all taken as 1.49445 here; and m_1, m_2 are the random numbers ranging from 0 to 1. In order to prevent the blind search, the generating velocities are locked in a certain range $[-v_{\max}, v_{\max}]$, and $v_{\max}$ is approximately taken as 10% of the search scope in the design space. $\omega(k)$ in (22) denotes the kth iterative weight factor and can be settled down with the following equation:

$$\omega(k) = \omega_s - (\omega_s - \omega_d)\left(\frac{k}{T_{\max}}\right), \tag{24}$$

where ω_s denotes the initial inertia weight whose recommended value is 0.9; ω_s is the inertia weight of the maximum iteration whose recommended value is 0.4; and $T_{\max}$ is the number of the maximum iterations, as it is taken as 200 here.

To find out the maximum value of the objective function in (20), the calculation process of PSO algorithm is as follows:

(a) Initialize the velocity and the location of the particles. Calculate the fitness of each particle by using the objective function, and find out P_{best} and G_{best}.

(b) Continue to move and search for the optimal solution in the search area. For the particles,

  (1) calculate the new tentative velocity with (23);
  (2) calculate the new location with (22);
  (3) calculate the new fitness of each particle, and then, accordingly, update the P_{best}.

(c) Update G_{best} by the judgement of the newly calculated P_{best}.

(d) If the stopping criteria are reached, output P_{best}; otherwise, go to the second step.

To make a much clearer description of the design process, the flow chart of the design approach with PSO is given in Figure 3 along with the solution of *Constraint II*. To verify the effectiveness of the PSO algorithm, the test functions in APPENDIX B are executed with the code here, and the results are listed in Fig S. 1 of APPENDIX B.

3.3. Constraint II and the Deduced Solution

3.3.1. Introduction of Constraint II. To accelerate the design process of *Constraint I* and get the explicit design expression for the meridional channel in engineering, a simpler assumption indicating that the chord length $|\mathbf{SH}|$ equals the enveloping circle's diameter in Figure 1 is proposed here. Therefore,

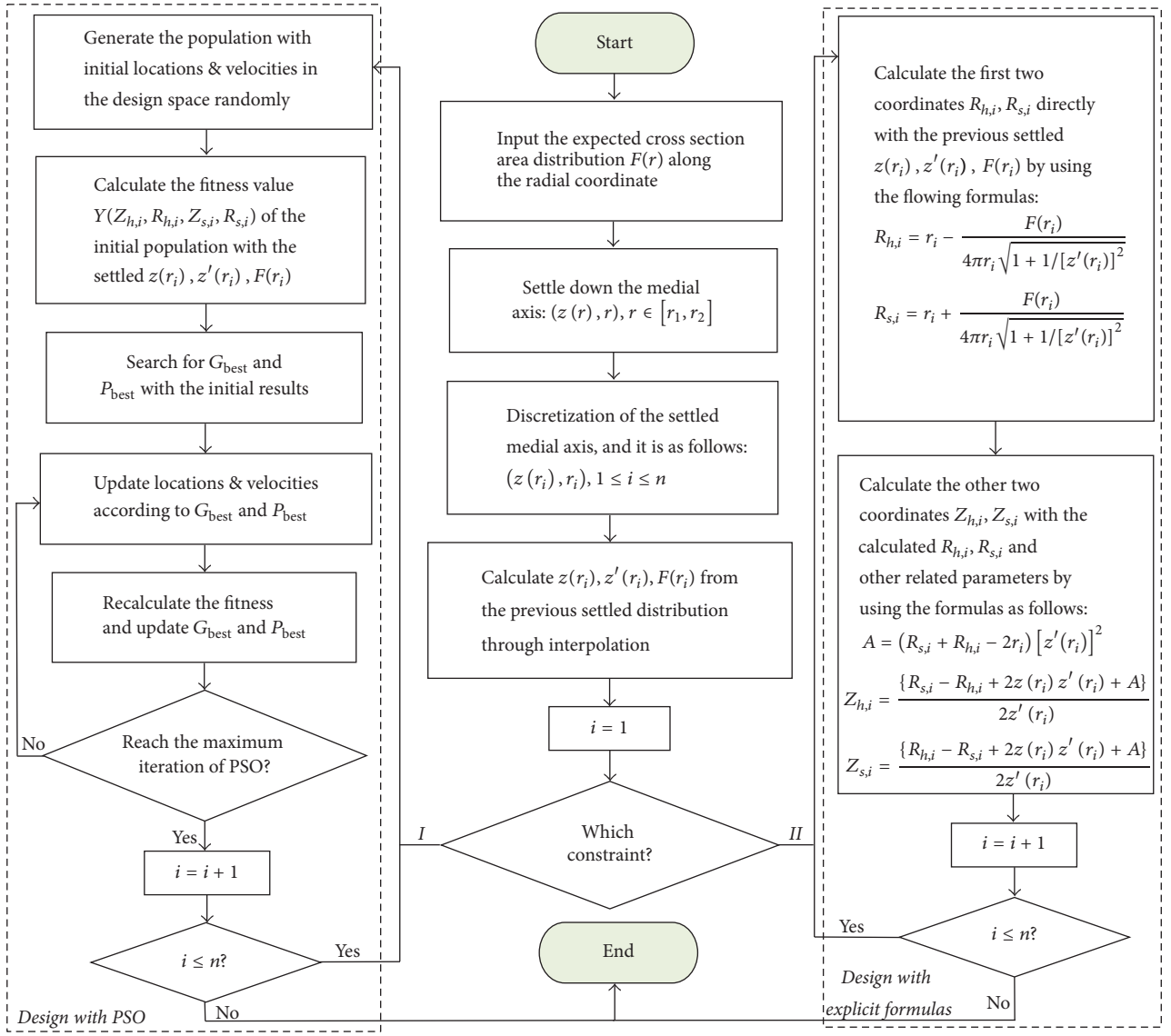

Figure 3: The sketch presentation of the new approach in the design cases.

the envelope circle's center **M** becomes the midpoint of |**SH**|. This simplifying assumption can be briefly expressed with the following mathematical equations:

$$z(r) \approx \frac{1}{2}(Z_s + Z_h) \tag{25}$$

$$r \approx \frac{1}{2}(R_s + R_h). \tag{26}$$

With this assumption, the expressions calculating the coordinates of the meridional channel would be derivated.

3.3.2. Deviation of the Explicit Expressions. From (13), the following equation could be got as

$$Z_h - Z_s = \frac{R_s - R_h}{z'(r)}. \tag{27}$$

And then with (25), (26), and (27), the cross section area equation of (16) can be transformed as

$$F(r) = 2\pi r \sqrt{1 + \frac{1}{(z'(r))^2}}\,(R_s - R_h). \tag{28}$$

Continually, with the combination of (15) and (26)~(28), the deduced explicit expressions used to settle down the design variables are as follows:

$$R_h = r - \frac{F(r)}{4\pi r \sqrt{1 + 1/[z'(r)]^2}}$$

$$R_s = r + \frac{F(r)}{4\pi r \sqrt{1 + 1/[z'(r)]^2}}$$

$$Z_h = \frac{\left\{R_s - R_h + 2z(r)\,z'(r) + \left(R_s + R_h - 2r\right)\left[z'(r)\right]^2\right\}}{2z'(r)}$$

$$Z_s = \frac{\left\{R_h - R_s + 2z(r)\,z'(r) + \left(R_s + R_h - 2r\right)\left[z'(r)\right]^2\right\}}{2z'(r)}, \quad (29)$$

where r, $z(r)$, $z'(r)$ are the prescribed variables, and their settlement is shown in APPENDIX A; $F(r)$ can be given previously or calculated by using (12) from the other related variables.

4. Design Cases to Verify the Feasibility of the New Approach

As for the established new approach in Section 3, the specific design process for its application in engineering is shown in Figure 3. In the design process, controlled by the discrete medial axis from the inlet to the outlet, the related coordinates determining the meridional channel are designed with the new approach of different constraints *(Constraint I or II)*.

To explore the effectiveness of the meridional design approach proposed above, the typical structures from the previous studies are adopted here to be the design targets, and the redesign results with the new approach are evaluated by comparison of the targets. Specific details for the application of the new approach in different conditions would be discussed next.

4.1. Meridional Shape Design for the Centrifugal Pump. Constructed with the linear lines and circular arcs, a series of meridional channels with good performance are designed based on the ISO 2858-1975 in [11]. Those pumps' specific speeds are ranging from 0.11 to 0.97, and they have similar structures. We take one typical structure as the design target, whose working conditions are listed as follows: the volume flow is $Q = 100\,\mathrm{m}^3/\mathrm{h}$; the head is $H = 43\,\mathrm{m}$; and the rotational speed is $n = 2900$ rpm. As for the meridional shape of this typical pump, Zou et al. [13] have already extracted the medial axis $(z(r), r)$ and the distribution of the cross section area $F(r)$ in their study, which are shown in Figure 4.

At first, *Constraint I* solved with PSO algorithm is applied in the design process. As for the identified medial axis, it is discretized into 24 points which are marked as $P_1, P_2, \ldots, P_{24}$. Based on the previous settled distribution, the related design variables $z(r_i), F(r_i)$ $(1 \le i \le 24)$ of the 24 points can be got through fitting and interpolation, whose final results are also given in Figure 4. And then with the application of the design flow chart shown in Figure 3, the corresponding design coordinates controlled by the 24 points are calculated from one point to another. Consequently, the evolutionary generations of the design process are shown in Figure 5(a), and it is found out that the related objective functions get close to 0 just within 200 generations, which means that the

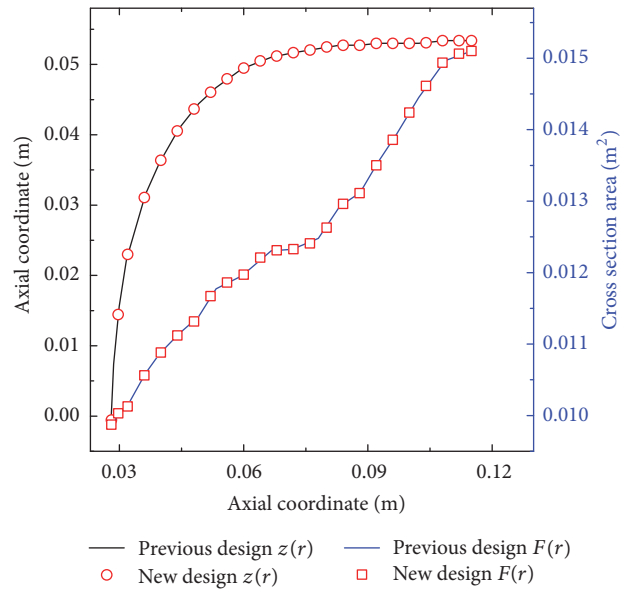

Figure 4: Initial design variables extracted from the previous design [13].

new design results are well in accord with (15)~(17), and they are just the design coordinates we are searching for. Plus, in Figure 5(b), the final design results are presented along with the previous structure constructed with linear lines and circular arcs (marked with red lines in the figure), and in the figure, it is verified that the new design approach based on *Constraint I* can well capture the meridional contours and fit in well with the previous design.

After verifying the effectiveness of *Constraint I* in the design process, *Constraint II* and the deduced explicit expressions of (29) are then applied in the design process. In correspondence to the same 24 discretized control points on the medial axis above, the new design results are shown in Figure 6. In comparison with the previous design result, it is known that the new design fits in well with the previous design except for the minor error at the turning section (in the marked box of Figure 6), which would be further discussed in Section 5.1.

To compare the aerodynamic parameters between the new design results and the target, the 3D meridional channels which are got by rotating the designed 2D profiles around the axial coordinate are simulated and analyzed. The parameters of the blade are not given in the reference, and the main focus is about the meridional shape design here, so that the simulation of the meridional channels without the installation of the blades is conducted here.

With the generated configurations and the working conditions proposed above, the inner flows are then simulated with the CFX solver. For the setup of the solver, the standard $k - \varepsilon$ turbulent model and the second-order upwind discretization are selected. Plus, to reach maximal $y+$ around 10 in the computational domains, the minimum height of the cells is controlled to be 0.06 mm at the walls.

Correspondingly, the computational domain and the simulating results about the static pressure and the relative

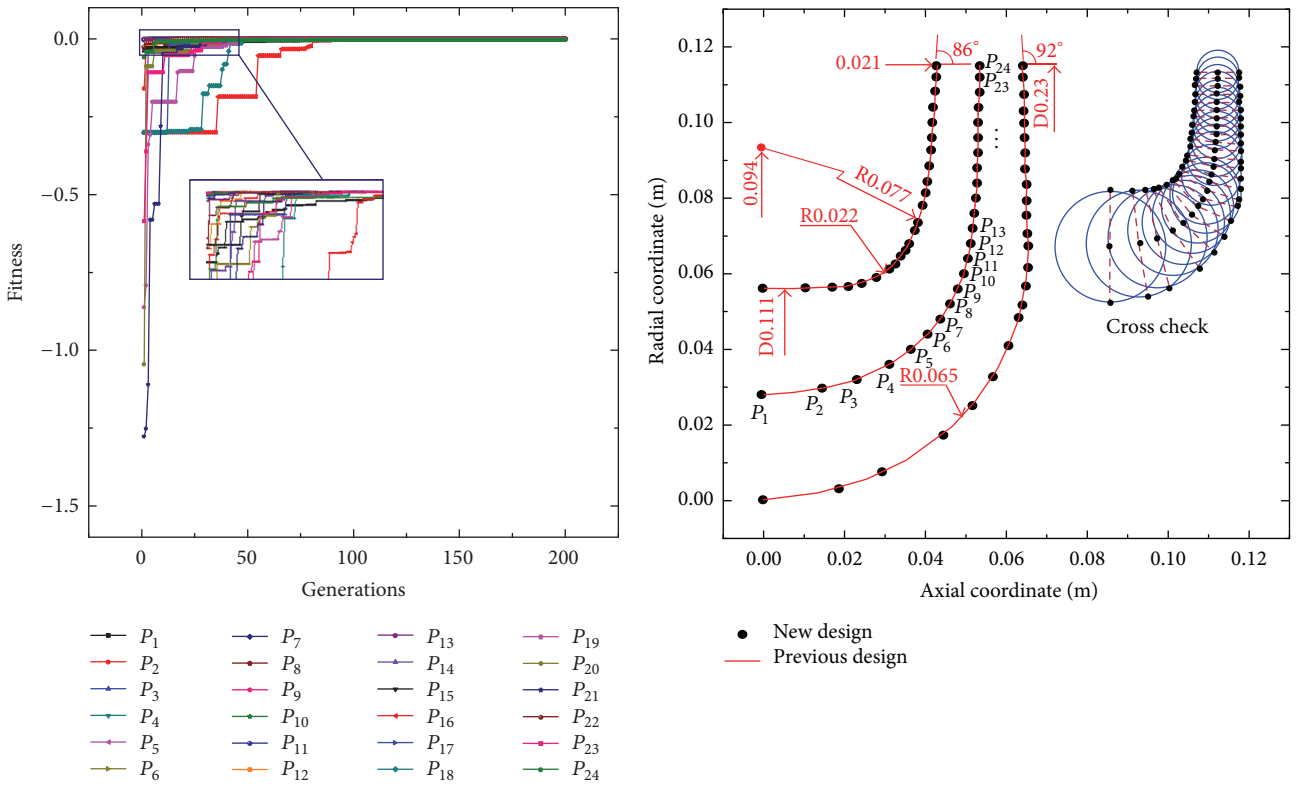

(a) The evolutionary generations in the design process

(b) Comparison between the new design result and the previous design

FIGURE 5: Application of *Constraint I* and PSO algorithm in the meridional channel design of the centrifugal pump.

velocity are presented in Figure 7. From the figure, it is known that there are almost no differences between the design results and the target; however, the design result with *Constraint I* is much more accurate than the result with *Constraint II*.

4.2. Meridional Shape Design for the Mixed-Flow Pump. The radial pumps consist of the centrifugal pump and the mixed-flow pump. After designing the meridional shape of the centrifugal pump, the new design approach is then applied to design the meridional shape of the mixed-flow pump.

The nuclear coolant pump AP1000 is a typical mixed-flow pump, and Wang [16] has designed its meridional shape with another method in his study before. This typical mixed-flow pump is then taken as the design target here, and the specific working conditions for the pump are as follows: the volume flow is $Q = 17880\,\mathrm{m}^3/\mathrm{h}$, the head is $H = 111\,\mathrm{m}$, and the rotational speed is $n = 1800$ rpm. Moreover, the other related variables can be got from Wang's study, and the initial design variables are presented in Figure 8.

The medial axis here is discretized into 22 points from the inlet to the outlet. After the application of the design approach based on *Constraint I*, the corresponding design results are got and shown in Figure 9.

Continually, to explore the feasibility of *Constraint II*, the mathematical expressions of (29) are utilized to redesign the meridional shape, whose final design result is shown in Figure 10.

According to the design results in Figures 9(b) and 10, it is known that, similarly to the design results of the centrifugal pump, the new design approach established on these two kinds of constraints can well design the meridional contours of the mixed-flow pump in relation to the previous structure

Continually, to compare the characteristics of the inner flows between the new design results and the target, the meridional channels are then configured with the corresponding designed 2D profile.

Since the bladeless meridional channels have already been investigated in Figure 7, the situation that the meridional channels are installed with blades should also be considered. With the blade geometry provided by Xie et al. [21], the meridional channels containing seven blades are then to be simulated and investigated with CFD. The setup of the solver is the same as the description of Section 4.1. With the boundary conditions above, the simulating results are ultimately presented in Figure 11. The results denote that *Constraint I* solved with PSO is much more accurate than the explicit formulas of *Constraint II* in the design process, which is the same as the design results of the centrifugal pump.

5. Further Discussion

5.1. Comparison of the Two Constraints in the Design Approach. In order to identify the differences between the two kinds of constraints and evaluate their applicabilities, the

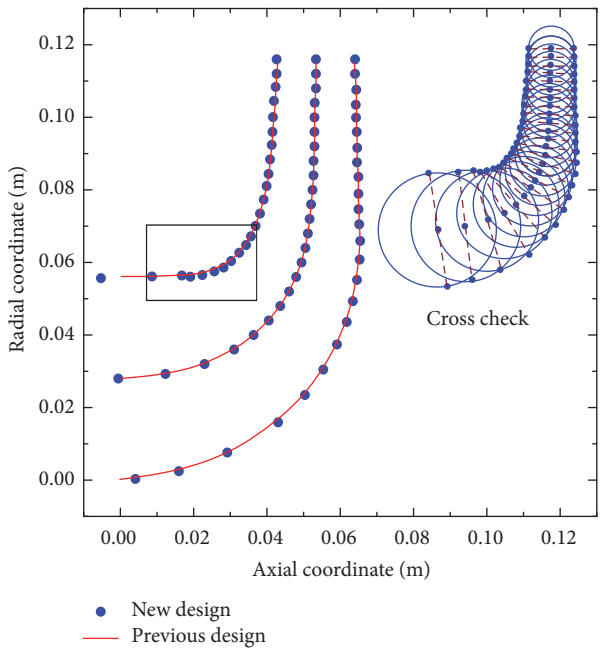

FIGURE 6: The new design result with the explicit expressions from *Constraint II*.

TABLE 1: Comparison of the constraints in the new design approach.

Constraints	Items	Centrifugal Pump	Mixed-flow Pump
Constraint I	$\overline{\delta}$ of the shroud	0.4%	0.16%
	$\overline{\delta}$ of the hub	1.5%	1.6%
	Design time	1481 s with 24 control points	0.304 s
Constraint II	$\overline{\delta}$ of the shroud	0.81%	0.21%
	$\overline{\delta}$ of the hub	2.6%	1.81%
	Design time	1139 s with 22 control points	0.202 s

related design results in Section 4 would be further analyzed. The design accuracy and the design time are chosen to be the analysis indexes.

To weigh the design accuracy quantitatively, the design error is imported and defined. As shown in Figure 12, the expression evaluating the design accuracy of the new design hub or shroud is given as

$$\overline{\delta} = \frac{1}{n}\sum_{i=1}^{n}\left|\frac{\Delta_i}{R_i}\right|, \tag{30}$$

where R_i is the radial coordinate of the previous hub or shroud; Δ_i is the difference between the new design and the previous design along the radial coordinate; and the value of n is taken as 5 here, and, as shown in Figure 12, the calculating points are of the same interval ($0.25L$) along the axial coordinate.

After recording the design time and calculating the design errors with (30), the analysis indexes of the design results are ultimately got and shown in Table 1.

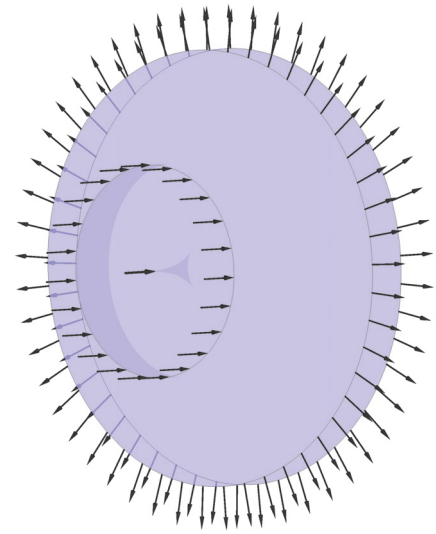

(a) The bladeless computational domain with a rotational speed of 2900 rpm

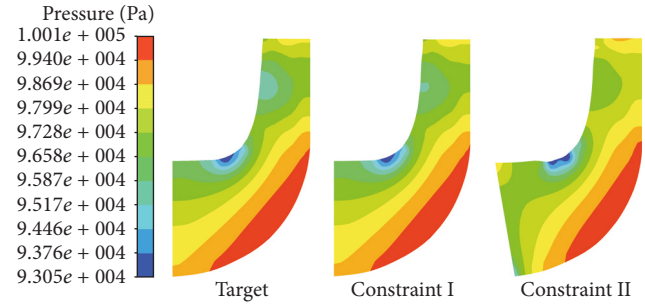

(b) Area averaged pressure distribution along the circumference

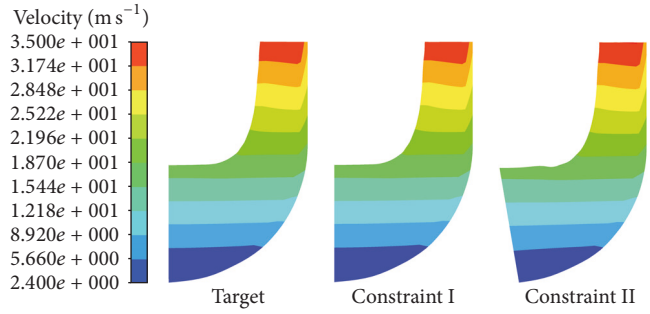

(c) Area averaged relative velocity distribution along the circumference

FIGURE 7: Comparison of the aerodynamic parameters between the design results and the target (without blades) for the centrifugal pump.

As for the design error δ, the closer it is to 0, the more accurate the design result will be. In the table, the design errors are ranging from 0.16% to 1.81%, which are close to 0, so that the design result could be quantitatively demonstrated to be desirable. As for the design errors of these two constraints, the related results with *Constraint I* are a little lower than the results with *Constraint II* in most of the conditions (0.4% < 0.81%, 1.5% < 2.6%, 0.16% < 0.21%, and 1.6% < 1.81%), so that the design approach with *Constraint I* is a little more accurate in designing the meridional shape.

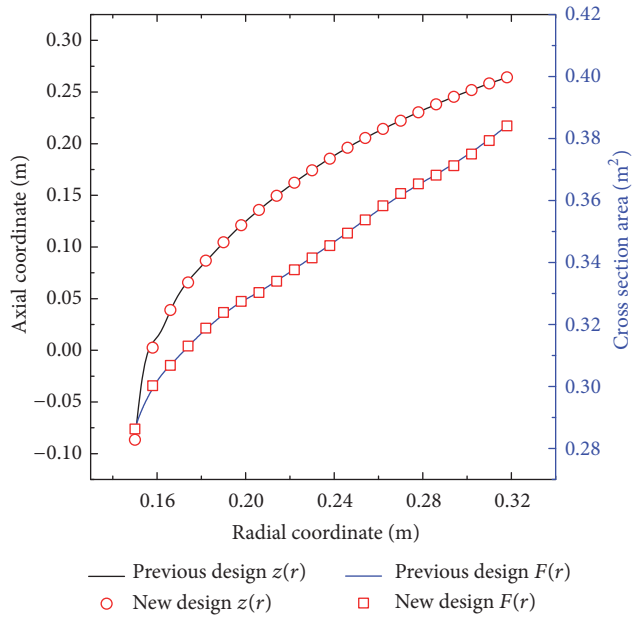

FIGURE 8: Initial design variables extracted from the previous design [16].

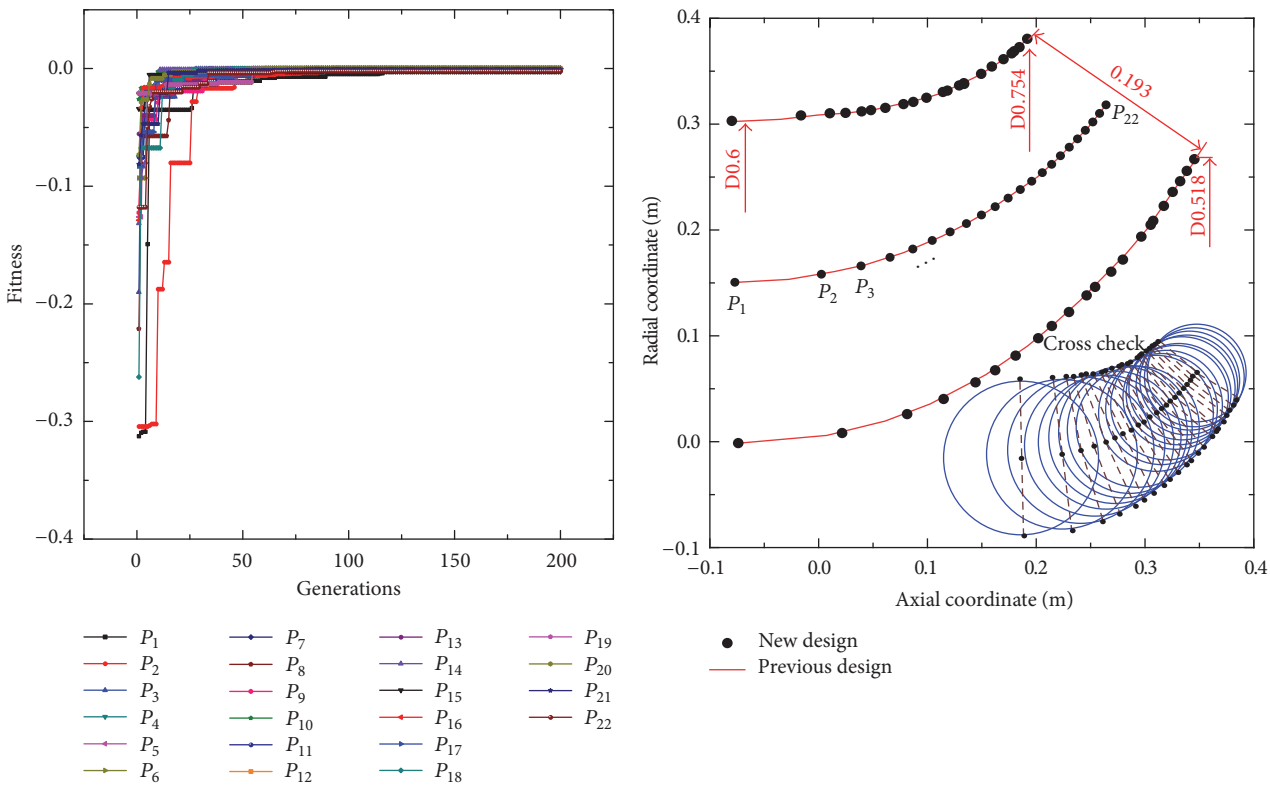

(a) The evolutionary generations in the design process

(b) Comparison between the new design result and the previous design

FIGURE 9: Application of *Constraint I* and PSO in the design process for the mixed-flow pump.

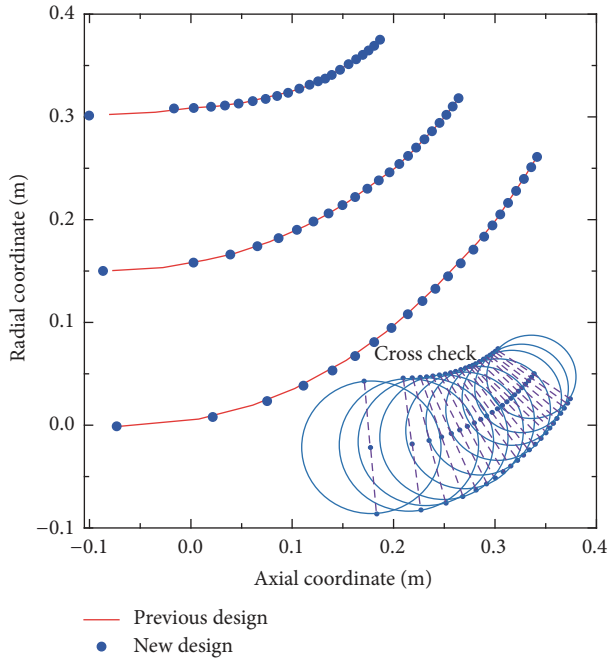

FIGURE 10: The new design result based on the explicit expressions of *Constraint II*.

The design process is conducted on the Dell station with an Intel Core i5-6500 CPU, whose clock speed is 3.2 GHz. As for the design with *Constraint I*, the total design time for the meridional channel of the centrifugal pump is 1481 s; namely, the corresponding average design time for one point on the medial axis is 1481/24 = 61.7 s. Also, the total time for designing the mixed-flow pump is 1139 s, so that, in correspondence with the 22 discretized points on medial axis, the average time generating a pair of coordinates on the hub and shroud contour lasts 1139/22 = 51.78 s. However, in terms of the total design time with *Constraint II*, it is just within 1 second. By comparison of these two constraints, it can be found that the design approach with *Constraint II* is much quicker.

5.2. Application of the New Design Approach in the Other Design Conditions. Instead of the cross section area, the distribution of the mean meridional velocity is taken as the initial design variable sometimes [15]; can the new design approach here deal with this kind of problem? Also, apart from its application in radial pump, can the new design approach here be applied in the other design area, for example, the impeller? To explore the possibility of these two conditions, the fan impeller in [14] is taken as the design target, and the meridional velocity $C_m(r)$ is given as the initial design variable, which is shown in Figure 13(a). According to the previous study, the blockage τ is ignored and taken as 1, the volume flow is 1.32 m^3/s, and the rotational speed is 2900 rpm. As a result, the distribution of $F(r)$ can be calculated with (12); then the final design results designed with *Constraint I* and *Constraint II* are presented in Figure 13(b). From the figure, it can be known that the new design approach with

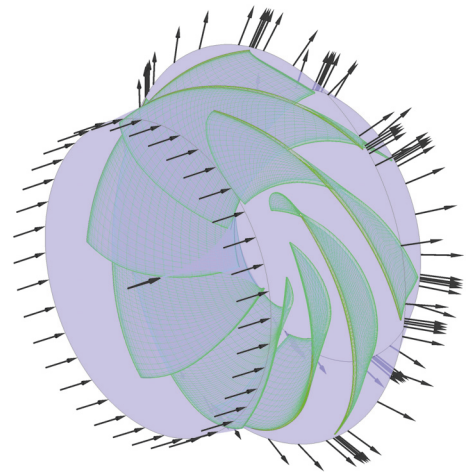

(a) The computational domain with a rotational speed of 1800 rpm

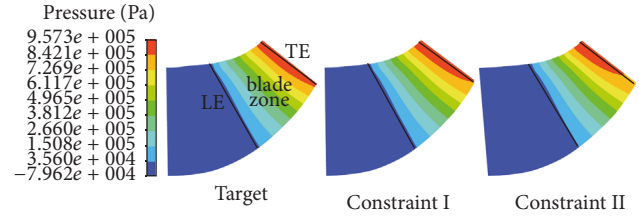

(b) Area averaged pressure distribution along the circumference

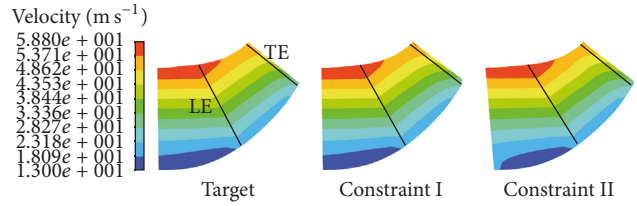

(c) Average relative velocity distribution along the circumference

FIGURE 11: Comparison of the aerodynamic parameters between the design results and the target (with blades) for the mixed-flow pump.

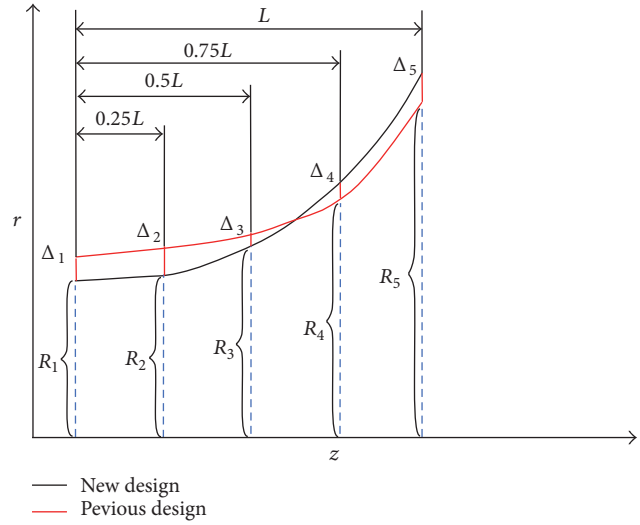

FIGURE 12: Definition of the design error for the design hub and shroud.

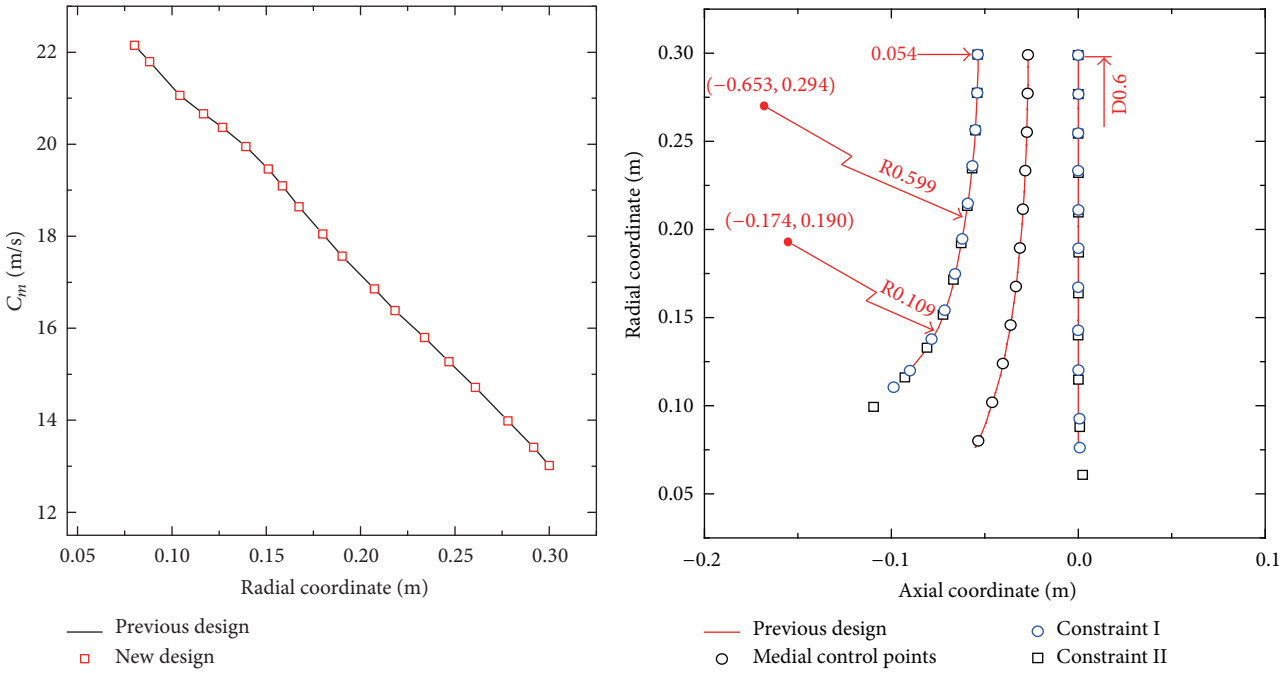

(a) The mean meridional velocity extracted from the previous study [14]

(b) Comparison between the new design results and the previous design

FIGURE 13: The fan impeller's meridional channel design with the new approach.

these two constraints can be well adaptable to the previous design. Moreover, the bladeless meridional channels are then to be simulated with the boundary conditions stated above, and from the distribution of the pressure and relative velocity in Figure 14, it can be further concluded that the proposed design approach can well design the meridional shape of the impeller by comparison with the previous design.

6. Conclusions and Future Work

6.1. Conclusions. The meridional channel is the foundation of the radial pump design, which was chosen from the database with lines and arcs in previous studies. To extend the design database and provide a simpler design approach in engineering, the new approach controlled by the medial axis is presented here. To verify the effectiveness of the new approach, it was applied to redesign some typical structures. The related conclusions in the study can be got as follows:

(1) Established on the simplified envelope formula, the circle equation, the cross section area equation, and another mathematical constraint, the new design approach can shape the meridional contours directly based on the medial axis contour and other settled variables. Instead of using the natural coordinate in previous studies, the new design approach sets r from the radial coordinate as the independent variable.

(2) Two kinds of separate solutions based on the corresponding mathematical constraints are presented in the design approach. For the first constraint *(Constraint I)*, the partial swarm optimization (PSO) algorithm was adopted to search for the suitable results in the design process. Furthermore, the second constraint *(Constraint II)* is imported, and the explicit mathematical expressions calculating the design points were finally got after a series of deviations.

(3) The effectiveness of the new approach was evaluated through designing the typical structures. When compared to the previous design, the design errors are ranging from 0.16% to 1.81%, which are close to 0, so that the feasibility of the new approach could be quantitatively demonstrated. Moreover, by comparison of the simulating aerodynamic parameters (pressure and relative velocity), the minor differences between the design results and the target can also illustrate the feasibility of the proposed design approach.

(4) In terms of the two constraints in the design approach, they have the separate advantages: the design approach with *Constraint I* is a little more accurate than *Constraint II* in designing the meridional shape; nevertheless, the latter is much simpler and can save a lot of time and computing resources in designing the meridional channel.

(5) Apart from the radial pump, the new approach presented here can also design the meridional shape of the impeller. In terms of the initial design variable with the cross section area, it can still be replaced by the mean meridional velocity in the design process.

6.2. Future Work. Peng et al. [7, 22] and Cao et al. [23] have already proposed the inverse blade design theory controlled by the distribution of the torque velocity, and a series of pumps working in different industrial areas have been got with the blade design theory. But there is a lack of a specific

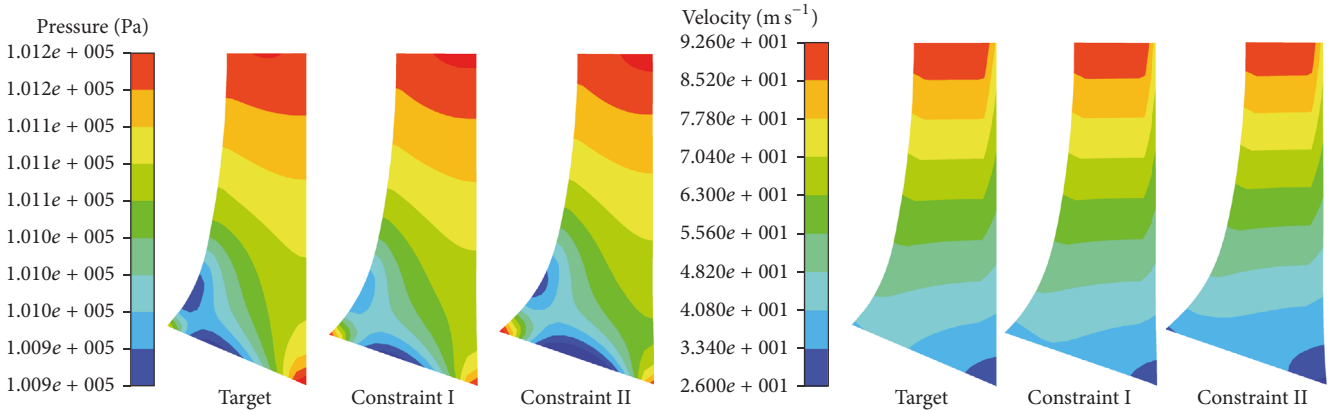

(a) Area averaged pressure distribution along the circumference

(b) Area averaged pressure distribution along the circumference

Figure 14: Comparison of the aerodynamic parameters between the design results and the target (without blades) for the vane.

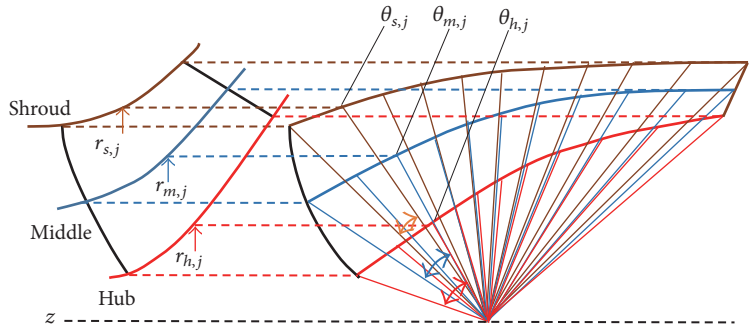

Figure 15: Sketch presentation of the pump design with the joint design methods.

meridional channel design approach to provide the skeleton and structural parameters for the inverse design of the blade. Therefore, we would try to do some joint works in the future; namely, with the combination of the newly proposed design approach and Peng-Cao's blade design theory, our future work would try to establish a pump inverse design platform which can design the good hydraulic meridional shape as well as the installed blade. Sketch presentation of the design process is briefly presented in Figure 15.

In the design platform of Figure 15, the meridional shape including the hub, the middle (or the medial axis), and the shroud contours is designed with the proposed method at first. Continually, the inverse design of the blade would then be conducted on the basis of the settled meridional contours.

Nomenclature

t:	Location in the natural coordinate
$\mathbf{p}$:	Tangent vector of the medial axis
$\mathbf{q}$:	Norm vector of the medial axis
θ:	Incline angle of the medial axis
$\mathbf{M}(z, r)$:	Control point on the medial axis
$\mathbf{S}(Z_s, R_s)$:	Designed coordinate on the shroud
$\mathbf{H}(Z_h, R_h)$:	Designed coordinate on the hub
d:	Diameter of the enveloping circle
C_m:	Mean meridional velocity
Q:	Volume flow
F:	Cross section area
Y:	Objective function of PSO
$h_{\min}, h_{\max}, s_{\min}, s_{\max}$:	The search range of PSO
$\mathbf{X}$:	The particles of PSO
$\mathbf{P}_i$:	P_{best} of PSO
$\mathbf{G}_i$:	G_{best} of PSO
ω:	Iterative weight factor of PSO
$T_{\max}$:	The maximum iteration number of PSO.

Conflicts of Interest

The authors declare that there are no conflicts of interest regarding the publication of this article.

Acknowledgments

This work is supported by National Basic Research Program of China (2015CB057301), Research and Innovation in Science and Technology Major Project of Liaoning Province (201410001), and Collaborative Innovation Center of Major Machine Manufacturing in Liaoning.

References

[1] J.-H. Kim, B.-M. Cho, S. Kim et al., "Design technique to improve the energy efficiency of a counter-rotating type pump-turbine," *Renewable Energy*, vol. 101, pp. 647–659, 2017.

[2] R. Tao, R.-F. Xiao, W. Yang, F. Wang, and W. Liu, "Optimization for cavitation inception performance of pump-turbine in pump mode based on genetic algorithm," *Mathematical Problems in Engineering*, vol. 2014, Article ID 234615, 9 pages, 2014.

[3] F.-J. Wang, L.-X. Qu, L.-Y. He, and J.-Y. Gao, "Evaluation of flow-induced dynamic stress and vibration of volute casing for a large-scale double-suction centrifugal pump," *Mathematical Problems in Engineering*, vol. 2013, Article ID 764812, 9 pages, 2013.

[4] R.-S. Zhu, Y. Liu, X. Wang, Q. Fu, A. Yang, and Y. Long, "The research on AP1000 nuclear main pumps' complete characteristics and the normalization method," *Annals of Nuclear Energy*, vol. 99, pp. 1–8, 2017.

[5] B.-S. Zhu, X.-H. Wang, L. Tan, D.-Y. Zhou, Y. Zhao, and S.-L. Cao, "Optimization design of a reversible pump-turbine runner with high efficiency and stability," *Renewable Energy*, vol. 81, pp. 366–376, 2015.

[6] M. Zangeneh, "A compressible three-dimensional design method for radial and mixed flow turbomachinery blades," *International Journal for Numerical Methods in Fluids*, vol. 13, no. 5, pp. 599–624, 1991.

[7] G.-Y. Peng, S.-L. Cao, M. Ishizuka, and S.-L. Hayama, "Design optimization of axial flow hydraulic turbine runner: Part I-an improved Q3D inverse method," *International Journal for Numerical Methods in Fluids*, vol. 39, no. 6, pp. 517–531, 2002.

[8] R.-F. Huang, X.-W. Luo, B. Ji et al., "Multi-objective optimization of a mixed-flow pump impeller using modified NSGA-II algorithm," *Science China Technological Sciences*, vol. 58, no. 12, pp. 2122–2130, 2015.

[9] H. Bing, S.-L. Cao, L. Tan, and B.-S. Zhu, "Effects of meridional flow passage shape on hydraulic performance of mixed-flow pump impellers," *Chinese Journal of Mechanical Engineering*, vol. 26, no. 3, pp. 469–475, 2013.

[10] M. V. Casey, "A computational geometry for the blades and internal flow channels of centrifugal compressors," *Journal of Engineering for Gas Turbines Power*, vol. 105, no. 2, pp. 288–394, 1983.

[11] X.-F. Guan, *Modern Pump Design Theory*, China Machine Press, Beijing, China, 2010.

[12] H.-I. Choi, S.-W. Choi, and H.-P. Moon, "Mathematical theory of medial axis transform," *Pacific Journal of Mathematics*, vol. 181, no. 1, pp. 57–88, 1997.

[13] J. Zou, P.-F. Wang, X.-D. Ruan, and F. Xin, "A statistical method on meridional profiles of centrifugal pumps," *Journal of Fluids Engineering, Transactions of the ASME*, vol. 134, no. 2, pp. 489–500, 2012.

[14] P.-F. Wang, X.-D. Ruan, J. Zou, and X. Fu, "Medial axis transform method for shape design of hub and shroud contours of impellers," *Journal of Fluids Engineering, Transactions of the ASME*, vol. 133, no. 3, Article ID 034502, 2011.

[15] Y. Wang, Q.-L. Dong, and Y. Zhang, "Meridional shape design and the internal flow investigation of centrifugal impeller," *Proceedings of the Institution of Mechanical Engineers, Part C: Journal of Mechanical Engineering Science*, vol. 8, no. 9, pp. 1–12, 2016.

[16] P. F. Wang, *Medial axis transform method for meridional shape design of pump impellers [Ph.D. thesis]*, Zhejiang University, 2013.

[17] H. Blum, "A transformation for extracting new descriptors of shape," *Models for the Perception of Speech Visual Form*, vol. 1967, no. 19, pp. 362–380, 1967.

[18] V. Srinivasan, L.-R. Nackman, J.-M. Tang, and S. N. Meshkat, "Automatic Mesh Generation Using the Symmetric Axis Transformation of Polygonal Domains," *Proceedings of the IEEE*, vol. 80, no. 9, pp. 1485–1501, 1992.

[19] H. Blum and R. N. Nagel, "Shape description using weighted symmetric axis features," *Pattern Recognition*, vol. 10, no. 3, pp. 167–180, 1978.

[20] J. Kennedy and R. Eberhart, "Particle swarm optimization," in *Proceedings of the IEEE International Conference on Neural Networks (ICNN '95)*, vol. 4, pp. 1942–1948, Perth, Western Australia, November-December 1995.

[21] R. Xie, S. T. Hao, and W. N. Jin, "Hydraulic model design and optimization of nuclear reactor coolant pump based on approximation model," *Journal of Engineering Thermophysics*, vol. 27, no. 7, pp. 1427–1431, 2016 (Chinese), (Chinese).

[22] G.-Y. Peng, "A practical combined computation method of mean through-flow for 3d inverse design of hydraulic turbomachinery blades," *Journal of Fluids Engineering, Transactions of the ASME*, vol. 127, no. 6, pp. 1183–1190, 2005.

[23] S.-L. Cao, G.-Y. Peng, and Z. Yu, "Hydrodynamic design of rotodynamic pump impeller for multiphase pumping by combined approach of inverse design and CFD analysis," *Journal of Fluids Engineering, Transactions of the ASME*, vol. 127, no. 2, pp. 330–338, 2005.